ISSN (Print) 1226-1750
ISSN (Online) 2233-6656
Journal of Magnetics 24(1), 10-16 (2019) https://doi.org/10.4283/JMAG.2019.24.1.010

Growth Condition Dependent Magnetic Properties of $CoFe_2O_4$ Nanoparticles and Their Highly T_2 Weighted Contrast in MRI

Qingbo Du[1,2]* and Qingyu Gao[2]

[1]*Wanbei Health Vocational College, Suzhou 234000, P. R. China*
[2]*College of Chemical Engineering, China University of Mining and Technology, Xuzhou 221116, P. R. China*

(Received 24 August 2018, Received in final form 5 January 2019, Accepted 5 January 2019)

In this work, we controlled the magnetic properties and water-solubility of $CoFe_2O_4$ nanoparticles by adjusting the reaction conditions during the preparation process. The growth condition-dependent crystalline, microstructure and therefore their magnetic properties were investigated in detail. It is found that the crystalline and the size of the nanoparticle become larger with the increasing of both the reaction temperature and reaction time. Consequently, the saturation magnetization (Ms) of our products was highly improved. Specifically, the typical sample prepared at 180 °C for 2 h, which has a higher Ms and good solubility in water was chosen as an alternative agent in magnetic resonance imaging The results show that it is an effective T_2 weighted MRI contrast agent.

Keywords : cobalt ferrite, nanoparticles, solvothermal method, magnetic resonance imaging

1. Introduction

Magnetic nanoparticles (such as Fe_3O_4, $CoFe_2O_4$, $NiFe_2O_4$ and γ-Fe_2O_3) have been investigated widely in recent years owing to their unique properties and a great potential application in magnetic resonance imaging (MRI) [1-4], hyperthermia [5, 6], drug delivery [7, 8], catalyst [9, 10] and Li ion battery [11, 12] *etc.*. Specially, they were extensively studied as a contrast agent in MRI. For a good contrast agents in MRI, magnetic nanoparticles must show a good chemical, physical and biological stability, moderate saturation magnetization, and high magneto crystalline anisotropy [13-21]. On the basis of this point, $CoFe_2O_4$ is an ideal candidate among all of the magnetic nanoparticles and thus attracts a wide research interest. For example, Cai *et al.* synthesized three-dimensional hierarchical $CoFe_2O_4$ porous microspheres through a template-free solvothermal route [22], which was used as a drug delivery carrier. Wang *et al.* [23] prepared monodispersed $CoFe_2O_4$ nanoparticles through a sonochemical route. The magnetic properties of $CoFe_2O_4$ nanoparticles were also investigated in detail. The *in vitro* cytotoxicity tests confirmed that the prepared $CoFe_2O_4$ nanoparticles had a negligible cytotoxicity and hold potential applications in biomedical fields. A lot of reports have confirmed that all of the size, morphology and magnetic properties of $CoFe_2O_4$ nanoparticles are growth condition-dependent [24-26]. Amirabadizadeh *et al.* reported that $CoFe_2O_4$ magnetic nanoparticles were prepared by a co-precipitation method [27]. The reaction time has an influence on their structures, morphologies and magnetic properties. Prabhakaran *et al.* [28] also demonstrated that the reaction temperature during their co-precipitation process has a great influence on their structures and magnetic behaviors. However, in spite of the significant progress for the magnetic properties of $CoFe_2O_4$ nanoparticles have been obtained, many technical restrictions associated with the colloidal stability and magnetic properties for practical applications are still a critical problem that should be overcome.

In this paper, we investigated the relationship between the growth conditions and the magnetic property of $CoFe_2O_4$ nanostructures. The growth-condition dependent structure, crystallinity and magnetic properties were studied in detail. It is found that the saturation Ms was changed greatly by varying the growth conditions. Among the products that we prepared under different condition, a sample with a moderate Ms and an excellent water solubility is obtained (prepared condition: keep the temperature at 180 °C for 2 h), which can be employed as a better contrast

*Corresponding author: Tel: +86-13665578650
Fax: +86-557-3095998, e-mail: qingbodu2008@sina.com

agent in MRI.We believed that the $CoFe_2O_4$ nanoparticles we prepared can be explored in the potential application in a more accurate detection and diagnosis.

2. Materials and Methods

2.1. Preparation of $CoFe_2O_4$ nanoparticles

All the chemicals used in the experiments were analytical grade without further purification.

In a typical synthesis, 0.6 g of PVP, 1 mmoL of $Co(NO_3)_2{\cdot}6H_2O$ and 2 mmoL of $Fe(NO_3)_3{\cdot}9H_2O$ were dissolved into 25 mL of ethylene glycol at magnetic stirring, followed by the addition of 5 mL of hydrazine hydrate (85 %) into the above orange solution to make a light brown homogeneous slurry. The slurry was transferred into a 50 mL of Teflon autoclave and heated at different reaction conditions. Six samples were prepared, namely CF1 to CF6, and summarized in Table 1. The $CoFe_2O_4$ nanoparticles was obtained by magnetic separation and washed several times with DI water and absolute ethanol after the autoclave was cooled down to room temperature. The collected samples were dried at 60 °C for 12 h for further use and characterization. The schematic diagram for solvothermal synthesis of the nanoparticles was illustrated in Figure 1.

2.2. Characterizations

The phase structures of the products were characterized by X-ray powder diffraction spectrometer on an XRD-6000 (Shimadzu Instruments, Japan). The morphology and microstructures of the as-prepared $CoFe_2O_4$ nanoparticles were obtained by scanning electron microscope (SEM, S-4800, Hitachi, Japan) with a 5 kV accelerating voltage and transmission electron microscope (TEM, Tecnai G20, FEI, Holland) with a 200 kV accelerating voltage. The X-ray photoelectron spectra (XPS) were collected on an ESCALab MKII X-ray photoelectron spectrometer, using monochromatized Mg Kα X-ray as the excitation source. Infrared spectra (IR) were recorded on NICOLET 5700 infrared spectrophotometer. The magnetic properties of the samples were measured by superconducting quantum interference device magnetometer (MPMS XL-7, Quantum Design, United states of America).

Table 1. Experimental conditions of different $CoFe_2O_4$ samples.

Samples No.	Temperature/°C	Time/h	Morphology
CF1	180	2	Nanoparticles
CF2	180	6	Nanoparticles
CF3	180	12	Nanoparticles
CF4	180	24	Nanoparticles
CF5	120	2	Nanoparticles
CF6	150	2	Nanoparticles

2.3. *In vitro* MRI experiments

The MRI tests were carried out on a MesoMR21-60H-I MRI scanner system at an ambient temperature. A certain amount of superparamagnetic $CoFe_2O_4$ nanoparticles was dispersed in distilled water to make aqueous solution with different concentration ranging from 0.005 to 0.156 mg mL^{-1}.

3. Results and Discussion

The phase of the samples were characterized by X-ray diffraction patterns. It is noted that the growth conditions will affect the morphology and thus the magnetic properties of the prepared samples [29-32]. In order to investigate this effect, experiment under different growth conditions were executed. The XRD patterns of the $CoFe_2O_4$ samples prepared at different growth conditions was shown in Fig. 2. It can be seen that all the diffraction peaks are well indexed to be the cubic structure of $CoFe_2O_4$ (JCPDS No. 22-1086). No any impurity was detected, which demonstrates that the prepared samples are high purity and crystallinity. In addition, the intensity of the diffraction peaks increased with the increasing of the reaction time, which indicates that the crystallinity of the prepared samples is also improved. The reaction temperature is another important factor which affects the structure, morphology and properties of the nanoparticles [28]. The XRD pattern of the samples prepared at different

Fig. 1. (Color online) Schematic of the solvothermal process that was utilized in the preparation of $CoFe_2O_4$ nanoparticles.

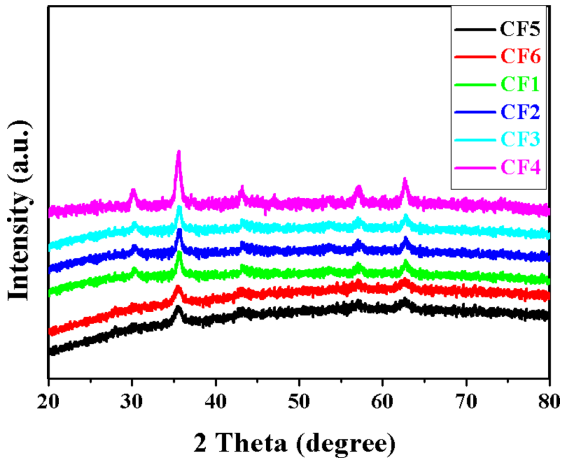

Fig. 2. (Color online) XRD patterns of the samples growth under different conditions.

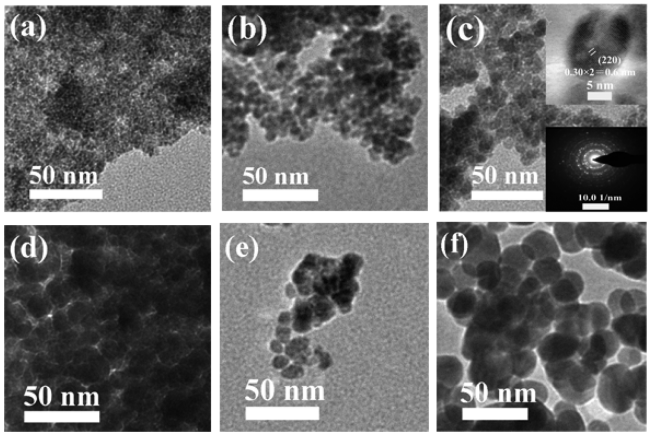

Fig. 3. TEM images of $CoFe_2O_4$ samples: (a): CF5, (b): CF6, (c): CF1, (d): CF2, (e): CF3, (f): CF4 (The insert in (c) are the HRTEM image of a single nanoparticle and the corresponding SAED).

temperatures while the reaction time was fixed at 2 h are well assigned to the cubic structure of $CoFe_2O_4$ (JCPDS No. 22-1086). The intensity of the diffraction peaks are increasing, while the width of the diffraction peaks is decreasing as the raise of the reaction temperature. These results confirmed that the size was increased and crystallinity was highly improved.

The morphologies of the $CoFe_2O_4$ nanoparticles prepared at different growth conditions were obtained using TEM imaging technique (Fig. 3). It can be seen that the samples show a sphere shape with an average diameter of about 20 nm. From Fig. 3, it can be seen that the size of the samples increased slightly with increasing of the reaction temperature and reaction time. The nanoparticles tend to aggregate due to their ultrasmall sizes and the interaction

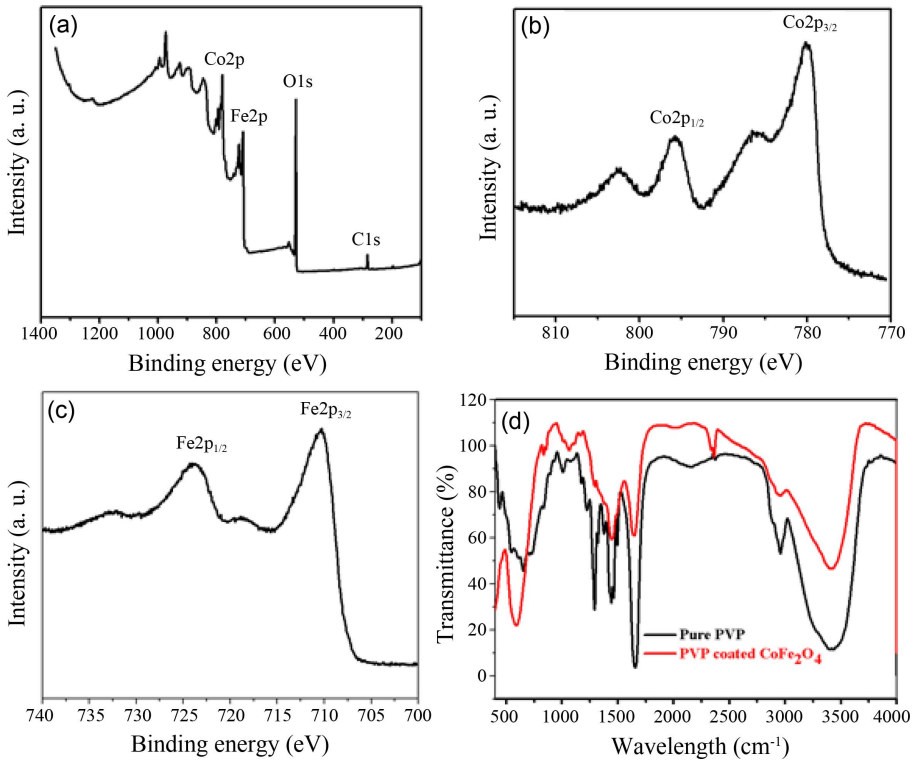

Fig. 4. (Color online) (a) XPS spectrums of CF1 sample, (b, c) high resolution XPS spectrum of Co2p and Fe2p and (d) FT-IR spectra of CF1 and pure PVP.

of magnetic force between different nanoparticles. In Fig. 3(c), the pattern inserted shows the HRTEM image of the CF1 sample, the crystal lattice was seen clearly, which confirmed that the samples have a good crystallinity. The lattice spacing was measured to be 0.30 nm, which corresponds to the value of (220) crystalline plane of $CoFe_2O_4$. Additionally, the SAED pattern demonstrates that the prepared $CoFe_2O_4$ nanoparticles were polycrystalline of cubic spinel crystal structure (the inserted in Fig. 3(c)). There were six diffraction rings from the center, which corresponding to (220), (311), (222), (400), (422), (511), (440) and (533) lattice planes of crystalline $CoFe_2O_4$, respectively.

The elemental composition and status of the $CoFe_2O_4$ nanoparticles were characterized by XPS, as shown in Fig. 4. The general profile of the $CoFe_2O_4$ nanoparticles indicate that the product are mainly composed of Co, Fe, O and C. The high resolution XPS spectra of Co and Fe were shown in Fig. 4(b)-(c). In the Co2p spectrum, there are four peaks centered at 780.1, 786.2, 795.7 and 802.5 eV, which could be assigned to Co2p3/2 and Co2p1/2, respectively (Fig. 4(b)) [22, 23, 33]. The spectrum of Fe2p was exhibited in Fig. 4(c). There are two main peaks located at 710.4 and 724.0 eV, which could be indexed to be Fe2p3/2 and Fe2p1/2, respectively. The results confirmed that the as-prepared sample was $CoFe_2O_4$, which are consistent with the previous study that conducted by XRD characterization.

The bonding status of PVP on the surface of the prepared $CoFe_2O_4$ nanoparticles was checked using a wavelength-dependent transmittance spectrum obtained by Fourier transformed infrared spectrum. There are five absorption bands for the pure PVP spectrum centered at around 3480, 2956, 1670, 1425 and 1281 cm^{-1}, which correspond to OH stretching, CH_2 asymmetric stretching, C=O symmetric stretching, CH_2 scissoring, C-N symmetric stretching, respectively (Fig. 4(d)) [34]. Two characteristic peaks centered at about 3480 cm^{-1} and 1670 cm^{-1} respectively slightly shift to lower frequency in the spectra of PVP coated $CoFe_2O_4$ nanoparticles, because of the interaction between PVP and $CoFe_2O_4$ nanoparticles [23]. The sharp peak centered at 587 cm^{-1} was assigned to Fe-O in the $CoFe_2O_4$ nanoparticles [35, 36]. The peak centered at 587 cm^{-1} was absent in pure PVP spectrum. The results reveal that the PVP polymer was coated on the surface of $CoFe_2O_4$ nanoparticles.

To further investigated the applications of our finding in MRI imaging, we first studied the magnetic properties of the samples that were prepared at different growth conditions (Fig. 5). The hysteresis loops of the prepared samples were all typical "S" shape, which implies that they all

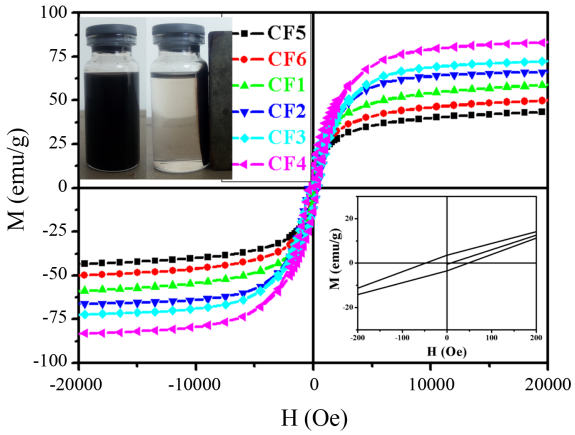

Fig. 5. (Color online) M-H hysteresis loops of different samples (the insert illustrates the digital photo of the $CoFe_2O_4$ nanoparticles with and without an external magnetic field).

have superparamagnetic properties. The saturation Ms, remnant magnetization (Mr) and coercivity (Hc) were summarized in Table 2. We can observe that the Ms, Mr and Hc of the samples increased with increasing solvothermal treatment duration. When the reaction time increased to 24 h, the saturation magnetization increased to 83.0 emu/g, which is nearly close to the value of pure bulk $CoFe_2O_4$ (94 emu/g) [18]. The decrease of Ms value may be caused by the existence of PVP, the small size of nanoparticles and the surface defect of nanoparticles [37]. When the reaction temperature evaluated from 120 to 180 °C, the Ms of the samples gradually increased from 43.6 to 58.5 emu/g, while the coercivity of the samples prepared at different temperature showed nearly zero Oe, respectively (Table 2). From the photo inserted in Figure 5, it is clearly to be seen that the obtained $CoFe_2O_4$ nanoparticles could suspend homogeneous in distilled water. However, the $CoFe_2O_4$ nanoparticles are absorbed to the wall when a magnet are put besides the wall of the vial. The suspension change into a nearly transparent solution, which shows that the prepared $CoFe_2O_4$ nanoparticles have strong magnetization. With high saturation Ms, the samples could be reached quickly to a cancerous site at an external magnetic field when used as a MRI agent. With a

Table 2. Magnetic properties of different $CoFe_2O_4$ samples.

Sample No.	Ms (emu/g)	Mr (emu/g)	Hc (Oe)
CF1	58.5	3.9	45.5
CF2	66.0	12.4	359.6
CF3	72.3	11.2	350.1
CF4	83.0	13.7	365.8
CF5	43.6	2.2	39.2
CF6	50.1	3.1	42.6

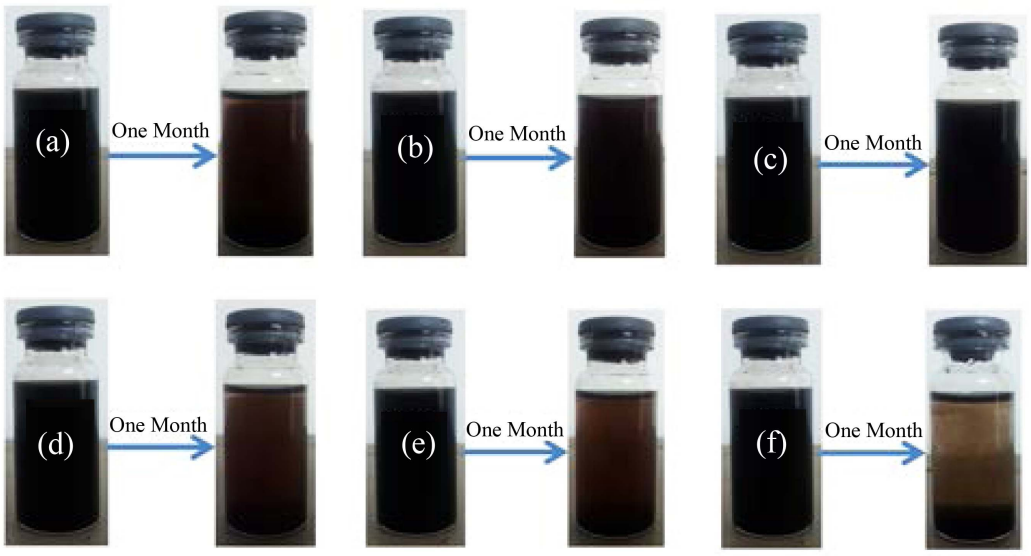

Fig. 6. (Color online) Dispersion stability test of PVP coated $CoFe_2O_4$ ((a) CF5, (b) CF6, (c) CF1, (d) CF2, (e) CF3, (f) CF4) nanoparticles in water.

relatively low remnant magnetization, the samples may be stable when the external magnetic field was removed. These properties are necessary for a MRI contrast agent.

The stability of the colloid is important for a MRI contrast agent [38]. We therefore investigated the stability of different samples, as shown in Fig. 6. The samples were dispersed into DI water, and put in air for one month. It can be seen that the CF1 has the best stability (Fig. 6c).

Based on the above results, we chosen the CF1 samples

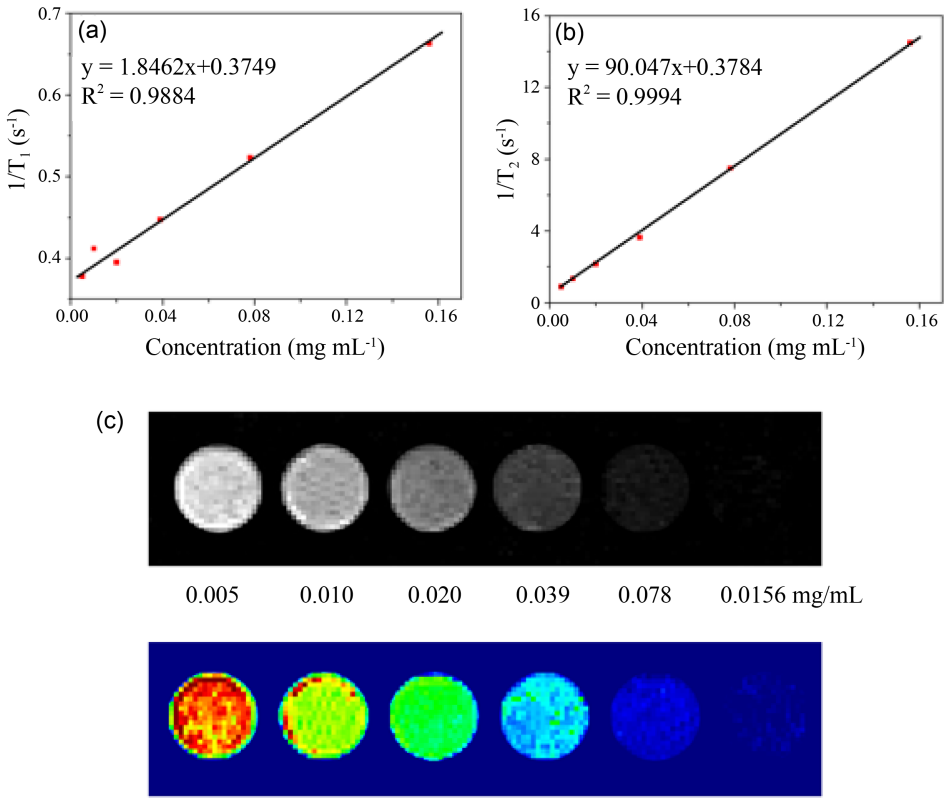

Fig. 7. (Color online) Plots of (a) $1/T_1$, (b) $1/T_2$ versus particle concentration and (c) T_2-weighted MRI photographs of CF1 dispersed in water at different concentrations.

to explore the MRI contrast effect in MesoMR21-60H-I scanner system at an ambient temperature. The relaxivity value of r_1 and r_2 was calculated to be 1.8462 and 90.047 mg mL^{-1} s^{-1} from the linearly plots in Fig. 7(a) and (b) respectively. The ratio of r_2/r_1 was 48.77, revealed that the as-prepared PVP coated $CoFe_2O_4$ nanoparticles may be a potential T_2-weighted contrast agent. From the color maps in Fig. 7(c), it is observed that the color of the maps changed from red to deep blue with the increase of the agent concentration. The results were in consistent with the observation of the grey maps as shown in Fig. 7(c). With increasing agent concentration, the color of grey maps changed from slight white to deep dark. It was confirmed that the PVP coated $CoFe_2O_4$ nanoparticles is a high T_2-weighted MRI agent.

4. Conclusions

In summary, $CoFe_2O_4$ magnetic nanoparticles coated with PVP were synthesized by a solvothermal route. A series of controlled experiments were carried out to investigate the influence of reaction time and temperature on the structure, morphology and magnetic properties of $CoFe_2O_4$ nanoparticles. The results demonstrated that the growth conditions had vital influences on their crystallinity and magnetic properties. The MRI experiments confirmed that the synthesized $CoFe_2O_4$ magnetic nanoparticles coated with PVP can enhance the MRI contrast effect and used as high efficient T_2 weighted contrast agent. This method can be used to synthesize other ferrites such as $MnFe_2O_4$ Fe_3O_4 $NiFe_2O_4$ and $ZnFe_2O_4$ *etc.*

Acknowledgements

This work was financially supported by Anhui province education department natural science research key project (No. KJ2018A0977) and the Fundamental Research Funds of the Central Universities (No. 2015XKZD09).

References

[1] Z. J. Zhou, C. Q. Wu, H. Y. Liu, X. L. Zhu, Z. H. Zhao, L. R. Wang, Y. Xu, H. Ai, and J. H. Gao, ACS Nano. **9**, 3012 (2015).
[2] P. Z. Li, P. Chevallier, P. Ramrup, D. Biswas, D. Vuckovich, M. A. Fortin, and J. K. Oh, Chem. Mater. **27**, 7100 (2015).
[3] H. Zhang, L. Li, X. L. Liu, J. Jiao, Ch. T. Ng, J. B. Yi, Y. E. Luo, B. H. Bay, L. Y. Zhao, M. L. Peng, N. Gu, and H. M. Fan, ACS Nano. **11**, 3614 (2017).
[4] Q. Zhang, T. Yin, G. Gao, J. G. Shapter, W. E. Lai, P. Huang, W. Qi, J. Song, and D. X. Cui, ACS Appl. Mater. Interfaces **9**, 17777 (2017).
[5] A. Cervadoro, M. Cho, J. Key, Ch. Cooper, C. Stigliano, S. Aryal, A. Brazdeikis, J. F. Leary, and P. Decuzzi, ACS Appl. Mater. Interfaces **6**, 12939 (2014).
[6] A. Walter, C. Billotey, A. Garofalo, C. Ulhaq-Bouillet, Ch. Lefèvre, J. Taleb, S. Laurent, L. V. Elst, R. N. Muller, L. Lartigue, F. Gazeau, D. Felder-Flesch, and S. Begin-Colin, Chem. Mater. **26**, 5252 (2014).
[7] M. Filippousi, S. A. Papadimitriou, D. N. Bikiaris, E. Pavlidou, M. Angelakeris, D. Zamboulis, H. Tian, and G. V. Tendeloo, Int. J. Pharm. **448**, 221 (2013).
[8] Z. Y. Cheng, Y. L. Dai, X. J. Kang,C. X. Li, S. S. Huang, H. Zh. Lian, Zh. Y. Hou, P. A. Ma, and J. L. Lin, Biomaterials **35**, 6359 (2014).
[9] H. Y. Zhu, R. Jiang, S. H. Huang, J. Yao, F. Q. Fu, and J. B. Li, Ceramics International **41**, 11625 (2015).
[10] G. Y. He, J. J. Ding, J. G. Zhang, Q. L. Hao, and H. Q. Chen, Industrial & Engineering Chemistry Research **54**, 2862 (2015).
[11] J. X. He, S. Y. Zhao, Y. P. Lian, M. J. Zhou, L. D. Wang, B. Ding, and S. Z. Cui, Electrochimica Acta. **229**, 306 (2017).
[12] F. Maroni, S. Gabrielli, A. Palmieri, E. Marcantoni, F. Croce, and F. Nobili, J. Power Sources **332**, 79 (2016).
[13] Z. Zhang, Y. Z. Jiang, M. Q. Chi, Z. Z. Yang, G. D. Nie, X. F. Lu, and C. Wang, Applied Surface Science **363**, 578 (2016).
[14] Z. Z. Liu, S. J. Yang, Y. N. Yuan, J. Xu, Y. F. Zhu, J. J. Li, and F. Wu, J. Hazard. Mater. **324**, 583 (2017).
[15] Z. Huang, B. Chi, L. Jian, S. Y. Yi, and Y. Q. Liu, J. Alloys Compd. **695**, 3435 (2017).
[16] Y. F. Zhu, X. B. Lv, L. L. Zhang, X. D. Guo, D. J. Liu, J. J. Chen, and J. Y. Ji, Electrochimica Acta. **215**, 247 (2016).
[17] V. Georgiadou, G. Makris, D. Papagiannopoulou, G. Vourlias, and C. Dendrinou-Samara, ACS Appl. Mater. Interfaces **8**, 9345 (2016).
[18] H. X. Wu, G. Liu, X. Wang, J. M. Zhang, Y. Chen, J. L. Shi, H. Yang, H. Hu, and S. P. Yang, Acta Biomaterialia. **7**, 3496 (2011).
[19] V. Georgiadou, V. Tangoulis, I. Arvanitidis, O. Kalogirou, and C. Dendrinou-Samara, J. Phys. Chem. C **119**, 8336 (2015).
[20] R. Vecchione, V. Quagliariello, P. Giustetto, D. Calabria, A. Sathya, R. Marotta, M. Profeta, S. Nitti, N. Silvestri, T. Pellegrino, R. V. Iaffaioli, and P. A. Netti, Nanomedicine: Nanotechnology, Biology and Medicine **13**, 275 (2017).
[21] Y. He, Y. Wang, X. Yang, S. B. Xie, R. Yuan, and Y. Q. Chai, ACS Appl. Mater. Interfaces **8**, 7683 (2016).
[22] B. Cai, M. G. Zhao, Y. Ma, Z. Z. Ye, and J. Y. Huang, ACS Appl. Mater. Interfaces **7**, 1327 (2015).
[23] G. S. Wang, Y. Y. Ma, J. B. Mu, Z. X. Zhang, X. L. Zhang, L. Zhang, H. W. Che, Y. M. Bai, J. X. Hou, and H. L. Xie, Applied Surface Science **365**, 114 (2016).

[24] S. Haffer, T. Walther, R. Köferstein, S. G. Ebbinghaus, and M. Tiemann, J. Phys. Chem. C **117**, 24471 (2013).
[25] M. Zhong, P. Fei, X. R. Fu, Z. Q. Lei, and B. T. Su, Industrial & Engineering Chemistry Research **52**, 8230 (2013).
[26] D. Peddis, C. Cannas, A. Musinu, A. Ardu, F. Orru, D. Fiorani, S. Laureti, D. Rinaldi, G. Muscas, G. Concas, and G. Piccaluga, Chem. Mater. **25**, 2005 (2013).
[27] A. Amirabadizadeh, Z. Salighe, R. Sarhaddi, and Z. Lotfollahi, J. Magn. Magn. Mater. **434**, 78 (2017).
[28] T. Prabhakaran, R. V. Mangalaraja, J. C. Denardin, and J. A. Jimenez, Ceramics International **43**, 5599 (2017).
[29] Y. Stetsyshyn, J. Raczkowska, O. Lishchynskyi, A. Bernasik, A. Kostruba, K. Harhay, H. Ohar, M. M. Marzec, and A. Budkowski, ACS Appl. Mater. Interfaces **9**, 12035 (2017).
[30] N. U. Patel, C. A. Purser, R. C. Baker, and A. V. Janorkar, Biomacromolecules **14**, 2891 (2013).
[31] X. L. Li, W. J. Wei, S. Z. Wang, L. Kuai, and B. Y. Geng, Nanoscale **3**, 718 (2011).
[32] C. V. Thulasi-Varma, C. V. V. M. Gopi, S. S. Rao, D. Punnoose, S. K. Kim, and H. J. Kim, J. Phys. Chem. C **119**, 11419 (2015).
[33] C. Wan, and J. Li, Carbohydrate Polymers **134**, 144 (2015).
[34] H. K. Wang, X. Lu, J. Tucek, J. G. Zheng, G. Yang, R. Zboril, and C. M. Niu, Electrochimica Acta. **211**, 636 (2016).
[35] X. A. Fan, J. G. Guan, X. F. Cao, W. Wang, and F. Z. Mou, Eur. J. Inorg. Chem. **3**, 419 (2010).
[36] S. L. Zhang, Q. Z. Jiao, J. Hu, J. J. Li, Y. Zhao, H. S. Li, and Q. Wu, J. Alloys Compd. **630**, 195 (2015).
[37] M. Filippousi, M. Angelakeris, M. Katsikini, E. Paloura, I. Efthimiopoulos, Y. Wang, D. Zamboulis, and G. V. Tendeloo, J. Phys. Chem. C **118**, 16209 (2014).
[38] Q. L. Jiang, S. W. Zheng, R. Y. Hong, S. M. Deng, L. Guo, R. L. Hu, B. Gao, M. Huang, L. F. Cheng, G. H. Liu, and Y. Q. Wang, Applied Surface Science **307**, 224 (2014).